

# Anisotropic superconductivity and Fermi surface reconstruction in the spin-vortex antiferromagnetic superconductor $\text{CaK}(\text{Fe}_{0.95}\text{Ni}_{0.05})_4\text{As}_4$

José Benito Llorens,<sup>1</sup> Edwin Herrera,<sup>1</sup> Víctor Barrena,<sup>1</sup> Beilun Wu,<sup>1</sup> Niclas Heinsdorf,<sup>2</sup> Vladislav Borisov,<sup>2,3</sup> Roser Valentí,<sup>2</sup> William R. Meier,<sup>4</sup> Sergey Bud'ko,<sup>4</sup> Paul C. Canfield,<sup>4</sup> Isabel Guillaumon,<sup>1</sup> and Hermann Suderow<sup>1</sup>

<sup>1</sup>*Laboratorio de Bajas Temperaturas y Altos Campos Magnéticos,*

*Departamento de Física de la Materia Condensada,*

*Instituto Nicolás Cabrera and Condensed Matter Physics Center (IFIMAC),*

*Unidad Asociada UAM-CSIC, Universidad Autónoma de Madrid, E-28049 Madrid, Spain*

<sup>2</sup>*Institut für Theoretische Physik, Goethe-Universität Frankfurt,*

*Max-von-Laue-Strasse 1, 60438 Frankfurt am Main, Germany*

<sup>3</sup>*Department of Physics and Astronomy, Uppsala University, Box 516, SE-75120 Uppsala, Sweden*

<sup>4</sup>*Ames Laboratory, Ames and Department of Physics & Astronomy, Iowa State University, Ames, IA 50011*

High critical temperature superconductivity often occurs in systems where an antiferromagnetic order is brought near  $T = 0\text{K}$  by slightly modifying pressure or doping.  $\text{CaKFe}_4\text{As}_4$  is a superconducting, stoichiometric iron pnictide compound showing optimal superconducting critical temperature with  $T_c$  as large as 38 K. Doping with Ni induces a decrease in  $T_c$  and the onset of spin-vortex antiferromagnetic order, which consists of spins pointing inwards to or outwards from alternating As sites on the diagonals of the in-plane square Fe lattice. Here we study the band structure of  $\text{CaK}(\text{Fe}_{0.95}\text{Ni}_{0.05})_4\text{As}_4$  ( $T_c = 10\text{ K}$ ,  $T_N = 50\text{ K}$ ) using quasiparticle interference with a Scanning Tunneling Microscope (STM) and show that the spin-vortex order induces a Fermi surface reconstruction and a fourfold superconducting gap anisotropy.

Iron pnictide superconductors mostly crystallize in a tetragonal structure. Optimal  $T_c$  appears in a phase diagram that shows structural, nematic or magnetic order in the vicinity of superconductivity[1–5]. Whereas most Fe-based superconductors need doping (or pressure) to reach maximal  $T_c$  values,  $\text{CaKFe}_4\text{As}_4$  is superconducting with the highest critical temperature in the pure stoichiometric compound with  $T_c \approx 38\text{ K}$ [6, 7]. Elastoresistivity, nuclear magnetic resonance (NMR) and neutron scattering experiments reveal magnetic fluctuations[8–10]. Contrary to other pnictide superconductors, there are neither structural modifications of the crystal when cooling nor strong electronic anisotropy in form of nematicity[7, 11]. The superconducting gap exchanges sign in different pockets of the Fermi surface and has  $s\pm$  symmetry as many other iron pnictides[12–15]. Electron count and other physical properties such as  $T_c$  and pairing symmetry are similar to the nearly optimally doped  $(\text{Ba}_{0.5}\text{K}_{0.5})\text{Fe}_2\text{As}_2$ [12, 16], where the magnetic order of  $\text{BaFe}_2\text{As}_2$  is suppressed by hole doping with K.

Following this idea, electron doping by substituting Fe with Co or Ni leads to antiferromagnetic order in  $\text{CaKFe}_4\text{As}_4$  (Fig. 1(a))[17]. The crystal structure is composed of  $\text{Fe}_2\text{As}_2$  layers that are separated alternatively with Ca and K. Thus, As sites in each layer are not equivalent, because their distance to the Fe plane differs due to being close either to Ca or to K. The distance between As1 and Ca is different than the distance between As2 and K (upper left inset in Fig. 1(a)). This eliminates the glide symmetry in the  $\text{Fe}_2\text{As}_2$  planes that exists in compounds such as  $\text{BaFe}_2\text{As}_2$ . As a consequence, antiferromagnetic order is non-collinear, with spins at each of the four Fe sites in the crystal structure pointing inwards to

(or outwards from) the As sites, giving a hedgehog spin-vortex crystal (SVC, brown arrows in upper left inset in Fig. 1(b))[17, 18]. The magnetic wavevector is the same as for the usual spin density wave antiferromagnetic or spin-charge magnetic order[18–21]. This SVC order produces a characteristic pattern of hyperfine fields at the As sites depicted in the inset of Fig. 1(b). The As1 sites have an alternating field up and down along the c axis (red circles and crosses). Critically, the hyperfine field is zero at As2 due to canceling contributions from surrounding Fe moments[17, 22]. There is robust experimental evidence for the presence of the SVC within the superconducting phase[17, 23–26]. However, the electronic band structure is yet unknown. Here we study the local density of states of  $\text{CaK}(\text{Fe}_{0.95}\text{Ni}_{0.05})_4\text{As}_4$  ( $T_{\text{SVC}} = 50\text{ K}$  and  $T_c = 10\text{ K}$ ) via Scanning Tunneling Microscopy (STM). We determine the band structure in the magnetic phase and show that the superconducting gap is highly anisotropic due to magnetism.

We study single crystals of  $\text{CaK}(\text{Fe}_{0.95}\text{Ni}_{0.05})_4\text{As}_4$  which have been obtained using the method of Ref.[11, 17]. Samples were mounted into a dilution refrigerator STM as described in Ref.[27]. We provide further details of crystals, low temperature cleaving mechanism and data analysis in Ref.[28].

Fig. 1(b) shows a typical surface obtained for  $\text{CaK}(\text{Fe}_{0.95}\text{Ni}_{0.05})_4\text{As}_4$  which resembles surfaces obtained in pure  $\text{CaKFe}_4\text{As}_4$ [13]. We identify atomically flat areas over a scanning window several  $\mu\text{m}$  in size, separated by atomic size trenches (black lines in Fig. 1(b)). Fig. 1(c) displays the tunneling conductance  $G = dI/dV$ . The superconducting gap manifests as the usual, strong reduction of the tunneling conductance for voltages of or

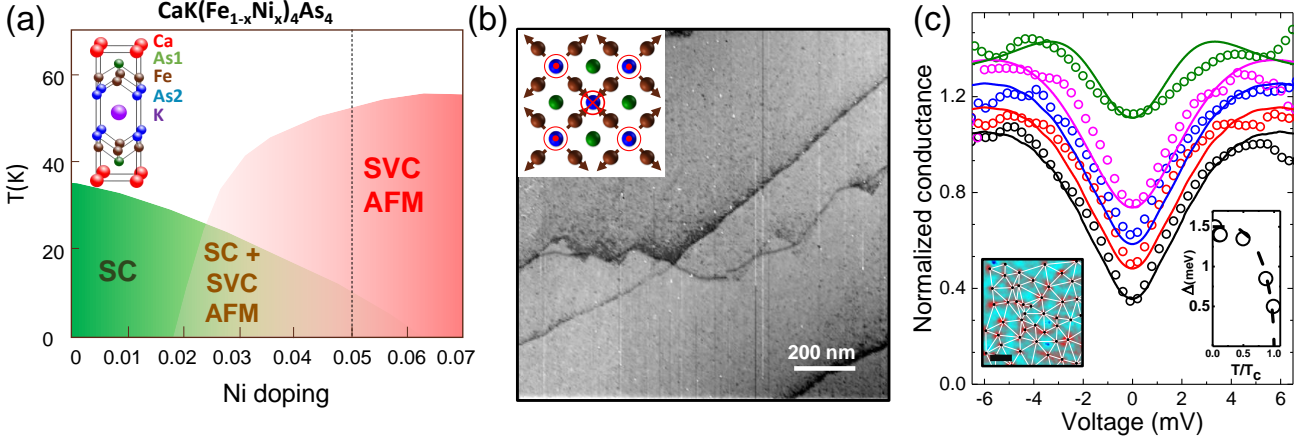


FIG. 1. (a) Schematic phase diagram of Ni doped  $\text{CaKFe}_4\text{As}_4$ , with a dashed vertical line indicating the Ni concentration discussed here. Crystalline structure of  $\text{CaK}(\text{Fe}_{0.95}\text{Ni}_{0.05})_4\text{As}_4$  is shown in the upper left inset. (b) STM topographic image of the surface of  $\text{CaK}(\text{Fe}_{0.95}\text{Ni}_{0.05})_4\text{As}_4$ . The difference between black and white corresponds to a height change of 0.3 nm. In the inset we show a view from the top of the structure, indicating Fe (brown) and As (As1 in blue and As2 in green) atoms and with arrows indicating the spin-vortex magnetic order. Note that the magnetic moments point towards As1, giving a finite hyperfine field pointing upwards along the c-axis (red circles with a cross) and from As1 atoms, giving a hyperfine field pointing downwards along the c-axis (red circle with a dot)[17]. At As2 the field cancels. (c) The temperature dependence of the tunneling conductance is shown as open circles in the main panel. Curves are taken (from bottom to top), at 0.3 K, 0.8 K, 1.4 K, 4 K and 7 K. Lines are fits using the density of states obtained for a distribution of value of the superconducting gap. The bottom right inset shows as black open circles the temperature dependence of the superconducting gap value, extracted from the maximum in the derivative of the density of states as a function of temperature normalized to  $T_c$ . The dashed line is a guide to the eye. Bottom left inset provides an image of the vortex lattice taken at 0.3 K and 2 T. Color scale shows the zero bias conductance which goes from the normal state value (red) to its value at zero field (blue). White lines are the Delaunay triangulation of vortex positions, which are shown as black dots. Black scale bar is 30 nm long. Further images and details are provided in Ref. [28].

der of a few mV, which disappears at about  $T_c$ . The zero bias density of states is finite and the coherence peaks are strongly smeared. Under magnetic fields we observed a disordered hexagonal vortex lattice (lower left inset of Fig. 1(c) and Ref.[28]). To estimate the superconducting gap at zero field in  $\text{CaK}(\text{Fe}_{0.95}\text{Ni}_{0.05})_4\text{As}_4$ , we construct a superconducting density of states  $N(E)$  allowing for a large distribution of values of the superconducting gap (details in Ref. [28]) which gives the tunneling conductance as solid lines in the main panel of Fig. 1(c). The lower right inset of Fig. 1(c) shows the energy at which the derivative of  $N(E)$ ,  $\frac{dN}{dE}$ , has a maximum. We obtain 1.5 meV at low temperatures, which is very similar to the gap value estimated from  $T_c \approx 10$  K,  $\Delta \approx 1.2$  meV. This value decreases with temperature as shown in the lower right panel of Fig. 1(c). These results are completely different from those observed in pure  $\text{CaKFe}_4\text{As}_4$ , where a two-gap structure with a few states at the Fermi level is found[12, 13].

When zooming into a small region we observe strong electronic scattering due to defects. The field of view shown in the topographic constant current image of Fig. 2(a)) is atomically flat. There are atomic size defects (black spots) and there is a wavy background. We can then build tunneling conductance maps  $G(V, x, y)$  at

each point  $(x, y)$  of the field of view. A representative example is shown in Figs. 2(b-f) for a few bias voltages  $V$ .  $G(V)$  is quite homogeneous and does not change much close to atomic size defects but we can identify clearly a wavy background whose wavelength changes with  $V$ . The contribution of scattered electrons to the  $G(V)$  is proportional to the densities of states of initial and final states, i.e. the joint density of states, and the scattering wavelength is equal to the difference  $q$  between initial and final scattering wavevectors[13, 29]. The Fourier transform of the tunneling conductance images is shown in Fig. 2(g-k). We identify three main scattering vectors,  $q_\alpha$ ,  $q_\beta$  and  $q_\gamma$ . The largest scattering vector,  $q_\gamma$ , is slightly anisotropic, being larger along the  $\bar{\Gamma}-\bar{X}$  direction than along  $\bar{\Gamma}-\bar{M}$  (notation of Brillouin zone directions follows the one proposed for pnictide superconductors in Ref.[30]). The Fourier amplitude at the three scattering vectors decreases close to the Fermi level due to the opening of the superconducting gap (Figs. 2(i)).

When plotting the bias voltage dependence of the scattering pattern along the high symmetry directions  $\bar{\Gamma}-\bar{X}$  and  $\bar{\Gamma}-\bar{M}$  (Figs. 3(a) and (b) respectively), we observe that all scattering vectors  $q$  decrease in size when increasing the bias voltage above the Fermi level. The qualitative behavior is very similar for both high sym-

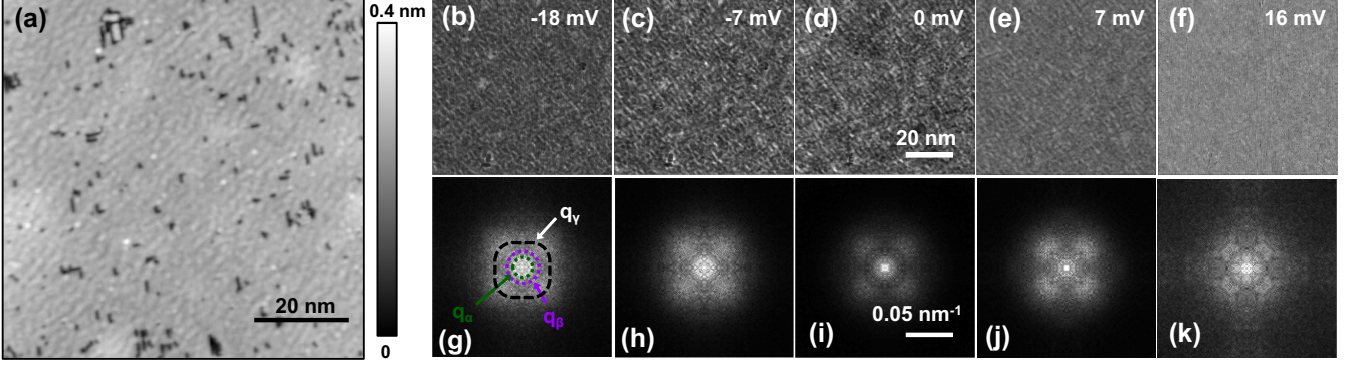


FIG. 2. (a) Topography of the area where we have made the quasiparticle interference experiment shown in (b-k). The color scale bar is given in the bottom right and the gray scale by the bar at the right. The image has been taken at a bias voltage of 30 mV and a current of 1 nA at zero magnetic field and at 0.3 K. (b-f) Tunneling conductance as a function of the position for a few representative bias voltages (given in each panel). The lateral scale bar is provided in (d). (g-k) Fourier transform, symmetrized taking into account the in-plane square lattice, of (b-f) shown in the first Brillouin zone. In (g) we mark the outer main scattering vector (black dashed circle) as well as the two inner scattering vectors (purple and green dashed circles). The lateral scale bar is given in (i) and grey scale goes from low (black) to large (white) scattering intensity.

metry directions, although the values of  $q_\gamma$  are slightly larger for  $\bar{\Gamma}-\bar{X}$  than for  $\bar{\Gamma}-\bar{M}$ . The reduction of the intensity inside the superconducting gap is band dependent. The superconducting gap is most clearly observed for the largest scattering vector  $q_\gamma$ .

In Fig. 3(c) we show the scattering intensity around zero bias and at  $q_\gamma$  as a function of the angle, with  $\theta = 0^\circ$  for  $\bar{\Gamma}-\bar{X}$  and  $\theta = 45^\circ$  for  $\bar{\Gamma}-\bar{M}$ . We find a fourfold modulation of the superconducting density of states which is not present in the stoichiometric compound and follows the symmetry of the SVC [12, 13]. The superconducting gap is larger along the direction where the hyperfine field on the As1 sites cancels ( $\bar{\Gamma}-\bar{X}$ , orange lines in Fig. 3(c)), whereas it is smaller when the hyperfine field remains finite ( $\bar{\Gamma}-\bar{M}$ , green lines in Fig. 3(c)), suggesting a competing scenario between superconductivity and magnetism. We will analyze this observation further below.

In what follows we investigate the origin of the three scattering vectors identified in Fig. 3(a,b). We have calculated the electronic structure of  $\text{CaKFe}_4\text{As}_4$  and  $\text{CaK}(\text{Fe}_{0.95}\text{Ni}_{0.05})_4\text{As}_4$  in the tetragonal paramagnetic phase within density functional theory as described in Ref. [28]. The effect of Ni doping has been taken into account with the Virtual Crystal Approximation (VCA). In Fig. 4(a) and (b) we show the respective Fermi surfaces. As expected, upon Ni doping the inner hole pockets slightly shrink in  $\text{CaK}(\text{Fe}_{0.95}\text{Ni}_{0.05})_4\text{As}_4$  (Fig. 4(b)) as compared to the pure compound (Fig. 4(a)) with the overall structure of the Fermi surface remaining similar. Our measurements (e.g. Fig. 3(a,b)) show, however, that the scattering pattern is very different. In  $\text{CaKFe}_4\text{As}_4$  [13] the scattering pattern consists of a single scattering vector, associated to interband scattering

between two hole bands centered at the Brillouin zone that increases strongly in size when increasing the bias voltage. In  $\text{CaK}(\text{Fe}_{0.95}\text{Ni}_{0.05})_4\text{As}_4$  there are three vectors whose size decreases much less drastically above the Fermi level. The SVC magnetic order invokes a folding of the band structure along the AFM wavevector due to the doubling of the unit cell (see inset in Fig. 4(c)). We assume that folding is the main consequence of the SVC in the bandstructure. The folded electron bands are shown in Fig. 4(c) and the Fermi surface in Fig. 4(d). The bands at the edges of the unfolded Brillouin zone are now centered around  $\bar{\Gamma}$ , providing a clearly defined set of bands coexisting in the same Brillouin zone region as the hole pockets centered at  $\bar{\Gamma}$ . In the calculated bands we identify three scattering vectors between hole and electron bands whose size corresponds to the observed  $q_\alpha$ ,  $q_\beta$  and  $q_\gamma$  vectors (arrows in Figs. 4(c,d)). Their value decreases with increasing bias voltage as is also found experimentally Fig. 3(a,b). Thus, the reconstructed Fermi surface provides an accurate description of the band structure of  $\text{CaK}(\text{Fe}_{0.95}\text{Ni}_{0.05})_4\text{As}_4$ .

We discuss now the observed fourfold modulation of the superconducting gap in  $\text{CaK}(\text{Fe}_{0.95}\text{Ni}_{0.05})_4\text{As}_4$  (Fig. 3(c)) which is not present in the stoichiometric compound [12, 13]. NMR experiments, Mössbauer spectroscopy and muon spin rotation/relaxation studies have shown evidence for the coexistence between superconductivity and the magnetic order in  $\text{CaK}(\text{Fe}_{0.95}\text{Ni}_{0.05})_4\text{As}_4$  [23–25]. It has been also reported that, similar to what is found in 122 compounds  $\text{Ba}_{1-x}\text{M}_x\text{Fe}_2\text{As}_2$  with  $\text{M} = \text{Co}, \text{Ni}$  and  $\text{Rh}$  [31–33] and  $\text{Ba}(\text{Fe}_{1-x}\text{K}_x)_2\text{As}_2$  [34], the ordered magnetic moment is gradually suppressed when entering in the superconduct-

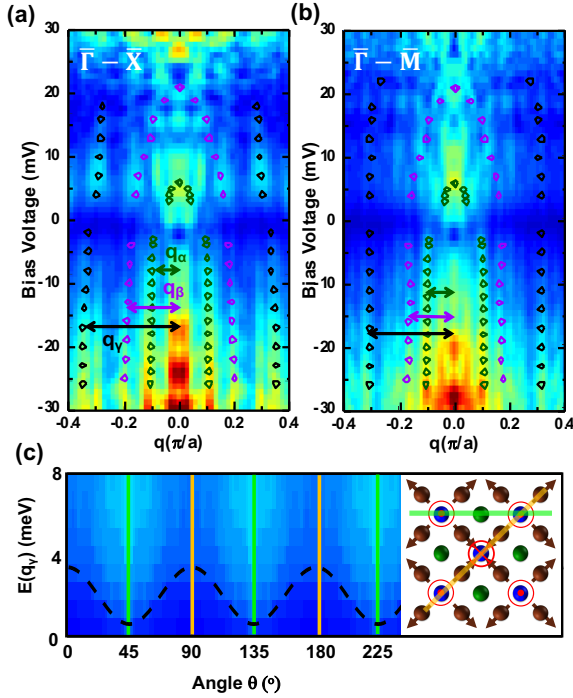


FIG. 3. (a) Scattering intensity for the two main symmetry directions,  $\Gamma-\bar{X}$  (left panel) and  $\Gamma-\bar{M}$  (right panel). Open circles mark the evolution of the scattering vectors with bias voltage. Scattering vectors  $q_\alpha$ ,  $q_\beta$  and  $q_\gamma$  are shown in black, violet and green. Color scale goes from low (blue) to high (red) scattering intensity. (b) Scattering intensity as a function of the angle with respect to the in-plane  $a$  axis for energies close to the Fermi level in  $q_\gamma$ . Color scale goes from blue (low intensity) to cyan (high intensity). The vertical light green and orange lines highlight the  $\Gamma-\bar{M}$  and  $\Gamma-\bar{X}$  directions respectively. The black dashed curve is a guide to the eye. The right inset shows a schematic representation of the lattice, with Fe atoms in brown (and their spins represented by arrows), As1 in blue and As2 in green and the main symmetry directions as light green and orange lines.

ing phase, suggesting that superconductivity and magnetism are competing for the same electrons in the iron-based superconductors[24–26, 35]. Our results show that this competition is also associated with the development of a strongly anisotropic superconducting gap.

The SVC phase is the only magnetic phase of pnictide superconductors where glide symmetry is broken within the unit cell. The relation between glide symmetry and superconductivity is not direct, because the coherence length is larger than the unit cell size. However, it may lead to a spin-current density wave, or  $d$ -density wave with increasing temperature or disorder[36]. The chiral properties of a spin-current density wave are connected to a pattern of currents inside the unit cell. The  $d$ -density wave has been suggested to be related to situations with hidden order parameters, such as the low temperature ordered phase of  $\text{URu}_2\text{Si}_2$  or the pseudogap in the cuprates[37–39]. By contrast to usual magnetic

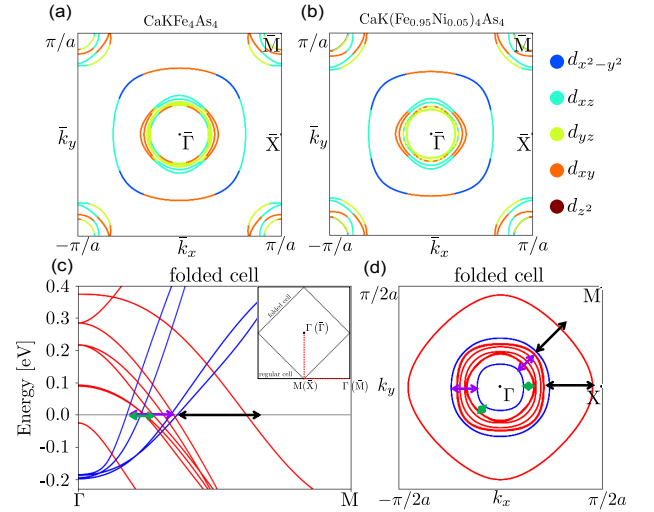


FIG. 4. Fermi surface of (a) pure  $\text{CaKFe}_4\text{As}_4$  and (b)  $\text{CaK}(\text{Fe}_{0.95}\text{Ni}_{0.05})_4\text{As}_4$  in the paramagnetic phase, obtained as described in the text. (c,d) Band structure and Fermi surface of  $\text{CaK}(\text{Fe}_{0.95}\text{Ni}_{0.05})_4\text{As}_4$  in the folded AFM Brillouin zone. Folded bands are shown in blue. Black, violet and green arrows are the main scattering vectors shown in Fig.3. Convention for the names of directions of folded and unfolded Brillouin zones (inset of (c)) follows Ref. [30].

fluctuations, which peak at horizontal directions on the Brillouin zone and favor repulsive interactions, fluctuations related to SVC peak at the corners of the Brillouin zone are attractive[36]. Thus, there are in principle no expected modifications of  $s\pm$  pairing in the SVC. However, the absence of local inversion symmetry, with the associated potential spin current  $d$ -density wave plaquette pattern is likely to have a strong influence on the superconducting properties and might produce the four-fold nodeless anisotropic gap observed here[36–39]. London penetration depth measurements in pure and electron irradiated crystals of  $\text{CaK}(\text{Fe}_{0.95}\text{Ni}_{0.05})_4\text{As}_4$  have suggested the presence of an anisotropic superconducting gap with  $s\pm$  symmetry which is more sensitive to disorder than in the stoichiometric compound [40]. This can also explain the observation of a finite density of states at zero bias in  $\text{CaK}(\text{Fe}_{0.95}\text{Ni}_{0.05})_4\text{As}_4$ .

In conclusion, we have measured the spatial dependence of the tunneling conductance in the SVC state of  $\text{CaK}(\text{Fe}_{0.95}\text{Ni}_{0.05})_4\text{As}_4$  and report direct evidence for a strong mutual influence between superconductivity and SVC antiferromagnetic order. Quasiparticle interference measurements supported by band structure calculations demonstrate a Fermi surface reconstruction and anisotropic pairing through an in-plane fourfold modulation of the superconducting gap. The comparison to  $\text{CaKFe}_4\text{As}_4$ , where there is no antiferromagnetic order and the superconducting gap shows no in-plane anisotropy, strongly suggests that the SVC antiferromagnetic state is responsible for the anisotropic pairing in



$\text{CaK}(\text{Fe}_{0.95}\text{Ni}_{0.05})_4\text{As}_4$ .

## ACKNOWLEDGMENTS

This work was supported by the Spanish Research State Agency (FIS2017-84330-R, RYC-2014-15093, CEX2018-000805-M), by the European Research Council PNICTEYES grant agreement 679080 and by EU program Cost CA16218 (Nanocohy-bri), by the Comunidad de Madrid through program NANOMAGCOST-CM (Program No. S2018/NMT-4321) and by the Deutsche Forschungsgemeinschaft (DFG, German Research Foundation) through TRR 288 - 422213477 (project A05). The research was supported by the U.S. Department of Energy (DOE), Office of Basic Energy Sciences, Division of Materials Sciences and Engineering. Ames Laboratory is operated for the U.S. DOE by the Iowa State University under Contract No. DE-AC02-07CH11358. WRM was supported by the Gordon and Betty Moore Foundations EPIQS Initiative through Grant GBMF4411. We acknowledge SEGAINVEX at UAM for design and construction of cryogenic equipment and the computational resources of the computer center of the Goethe University Frankfurt. We also thank R. Álvarez Montoya, S. Delgado and J.M. Castilla for technical support.

- 
- [1] Yoichi Kamihara, Takumi Watanabe, Masahiro Hirano, and Hideo Hosono, “Iron-based layered superconductor  $\text{La}[\text{O}1-x\text{F}x]\text{FeAs}$  ( $x = 0.05\text{--}0.12$ ) with  $T_c = 26\text{ K}$ ,” *Journal of the American Chemical Society* **130**, 3296–3297 (2008).
  - [2] Paul C. Canfield and Sergey L. Bud’ko, “FeAs-based superconductivity: A case study of the effects of transition metal doping on  $\text{BaFe}_2\text{As}_2$ ,” *Annual Review of Condensed Matter Physics* **1**, 27–50 (2010).
  - [3] Johnpierre Paglione and Richard L. Greene, “High-temperature superconductivity in iron-based materials,” *Nature Physics* **6**, 645 EP – (2010).
  - [4] P J Hirschfeld, M M Korshunov, and I I Mazin, “Gap symmetry and structure of Fe-based superconductors,” *Reports on Progress in Physics* **74**, 124508 (2011).
  - [5] Hideo Hosono and Kazuhiko Kuroki, “Iron-based superconductors: Current status of materials and pairing mechanism,” *Physica C: Superconductivity and its Applications* **514**, 399 – 422 (2015).
  - [6] Akira Iyo, Kenji Kawashima, Tatsuya Kinjo, Taichiro Nishio, Shigeyuki Ishida, Hiroshi Fujihisa, Yoshito Gotoh, Kunihiro Kihou, Hiroshi Eisaki, and Yoshiyuki Yoshida, “New-structure-type Fe-based superconductors:  $\text{CaAFe}_4\text{As}_4$  ( $A = \text{K, Rb, Cs}$ ) and  $\text{SrAFe}_4\text{As}_4$  ( $A = \text{Rb, Cs}$ ),” *Journal of the American Chemical Society* **138**, 3410–3415 (2016).
  - [7] W. R. Meier, T. Kong, U. S. Kaluarachchi, V. Taufour, N. H. Jo, G. Drachuck, A. E. Böhmer, S. M. Saunders, A. Sapkota, A. Kreyssig, M. A. Tanatar, R. Prozorov, A. I. Goldman, Fedor F. Balakirev, Alex Gurevich, S. L. Bud’ko, and P. C. Canfield, “Anisotropic thermodynamic and transport properties of single-crystalline  $\text{CaKFe}_4\text{As}_4$ ,” *Phys. Rev. B* **94**, 064501 (2016).
  - [8] W.-L. Zhang, W. R. Meier, T. Kong, P. C. Canfield, and G. Blumberg, “High- $T_c$  superconductivity in  $\text{CaKFe}_4\text{As}_4$  in absence of nematic fluctuations,” *Phys. Rev. B* **98**, 140501 (2018).
  - [9] J. Cui, Q.-P. Ding, W. R. Meier, A. E. Böhmer, T. Kong, V. Borisov, Y. Lee, S. L. Bud’ko, R. Valentí, P. C. Canfield, and Y. Furukawa, “Magnetic fluctuations and superconducting properties of  $\text{CaKFe}_4\text{As}_4$  studied by  $^{75}\text{As}$  NMR,” *Phys. Rev. B* **96**, 104512 (2017).
  - [10] Kazuki Iida, Motoyuki Ishikado, Yuki Nagai, Hiroyuki Yoshida, Andrew D. Christianson, Naoki Murai, Kenji Kawashima, Yoshiyuki Yoshida, Hiroshi Eisaki, and Akira Iyo, “Spin resonance in the new-structure-type iron-based superconductor  $\text{CaKFe}_4\text{As}_4$ ,” *Journal of the Physical Society of Japan* **86**, 093703 (2017).
  - [11] W. R. Meier, T. Kong, S. L. Bud’ko, and P. C. Canfield, “Optimization of the crystal growth of the superconductor  $\text{CaKFe}_4\text{As}_4$  from solution in the  $\text{FeAs}$ - $\text{CaFe}_2\text{As}_2$ - $\text{KFe}_2\text{As}_2$  system,” *Phys. Rev. Materials* **1**, 013401 (2017).
  - [12] Kyuil Cho, A. Fente, S. Teknowijoyo, M. A. Tanatar, K. R. Joshi, N. M. Nusran, T. Kong, W. R. Meier, U. Kaluarachchi, I. Guillaumon, H. Suderow, S. L. Bud’ko, P. C. Canfield, and R. Prozorov, “Nodeless multiband superconductivity in stoichiometric single-crystalline  $\text{CaKFe}_4\text{As}_4$ ,” *Phys. Rev. B* **95**, 100502 (2017).
  - [13] Antón Fente, William R. Meier, Tai Kong, Vladimir G. Kogan, Sergey L. Bud’ko, Paul C. Canfield, Isabel Guillaumon, and Hermann Suderow, “Influence of multiband sign-changing superconductivity on vortex cores and vortex pinning in stoichiometric high- $T_c$   $\text{CaKFe}_4\text{As}_4$ ,” *Phys. Rev. B* **97**, 134501 (2018).
  - [14] Daixiang Mou, Tai Kong, William R. Meier, Felix Lochner, Lin-Lin Wang, Qisheng Lin, Yun Wu, S. L. Bud’ko, Ilya Eremin, D. D. Johnson, P. C. Canfield, and Adam Kaminski, “Enhancement of the superconducting gap by nesting in  $\text{CaKFe}_4\text{As}_4$ : A new high temperature superconductor,” *Phys. Rev. Lett.* **117**, 277001 (2016).
  - [15] G.A. Ummarino, “Phenomenology of  $\text{CaKFe}_4\text{As}_4$  explained in the framework of four bands Eliashberg theory,” *Physica C: Superconductivity and its Applications* **529**, 50 – 53 (2016).
  - [16] D. Jost, J.-R. Scholz, U. Zweck, W. R. Meier, A. E. Böhmer, P. C. Canfield, N. Lazarević, and R. Hackl, “Indication of subdominant  $d$ -wave interaction in superconducting  $\text{CaKFe}_4\text{As}_4$ ,” *Phys. Rev. B* **98**, 020504 (2018).
  - [17] William R. Meier, Qing-Ping Ding, Andreas Kreyssig, Sergey L. Bud’ko, Aashish Sapkota, Karunakar Kothapalli, Vladislav Borisov, Roser Valentí, Cristian D. Batista, Peter P. Orth, Rafael M. Fernandes, Alan I. Goldman, Yuji Furukawa, Anna E. Böhmer, and Paul C. Canfield, “Hedgehog spin-vortex crystal stabilized in a hole-doped iron-based superconductor,” *npj Quantum Materials* **3**, 5 (2018).
  - [18] Mareike Hoyer, Rafael M. Fernandes, Alex Levchenko, and Jörg Schmalian, “Disorder-promoted  $C_4$ -symmetric magnetic order in iron-based superconductors,” *Phys. Rev. B* **93**, 144414 (2016).
  - [19] Xiaoyu Wang, Jian Kang, and Rafael M. Fernandes, “Magnetic order without tetragonal-symmetry-breaking in iron arsenides: Microscopic mechanism and spin-wave

- spectrum,” *Phys. Rev. B* **91**, 024401 (2015).
- [20] Morten H. Christensen, Jian Kang, Brian M. Andersen, Ilya Eremin, and Rafael M. Fernandes, “Spin reorientation driven by the interplay between spin-orbit coupling and Hund’s rule coupling in iron pnictides,” *Phys. Rev. B* **92**, 214509 (2015).
- [21] Q-P Ding, William R Meier, J Cui, Mingyu Xu, AE Böhmer, Sergey L Bud’ko, Paul C Canfield, and Yuji Furukawa, “Hedgehog spin-vortex crystal antiferromagnetic quantum criticality in  $\text{CaK}(\text{Fe}_{1-x}\text{Ni}_x)_4$  as revealed by NMR,” *Physical review letters* **121**, 137204 (2018).
- [22] W. Meier, Growth, properties and magnetism of  $\text{CaKFe}_4\text{As}_4$ . PhD thesis, Iowa State University, 2018, <https://lib.dr.iastate.edu/etd/16856>.
- [23] Q-P Ding, William R Meier, AE Böhmer, SL Bud’ko, Paul C Canfield, and Yuji Furukawa, “Nmr study of the new magnetic superconductor  $\text{CaK}(\text{Fe}_{0.951}\text{Ni}_{0.049})_4\text{As}_4$ : Microscopic coexistence of the hedgehog spin-vortex crystal and superconductivity,” *Physical Review B* **96**, 220510 (2017).
- [24] Sergey L Bud’ko, Vladimir G Kogan, Ruslan Prozorov, William R Meier, Mingyu Xu, and Paul C Canfield, “Coexistence of superconductivity and magnetism in  $\text{CaK}(\text{Fe}_{1-x}\text{Ni}_x)_4\text{As}_4$  as probed by  $^{57}\text{Fe}$  Mössbauer spectroscopy,” *Physical Review B* **98**, 144520 (2018).
- [25] Rustem Khasanov, Gediminas Simutis, Yurii G Pashkevich, Tatyana Shevtsova, William R Meier, Sergey L Bud’ko, Vladimir G Kogan, and Paul C Canfield, “Magnetism and its coexistence with superconductivity in  $\text{CaK}(\text{Fe}_{0.949}\text{Ni}_{0.051})_4\text{As}_4$ : muon spin rotation/relaxation studies,” *Phys. Rev. B* **102**, 094504 (2020).
- [26] Andreas Kreyssig, John M Wilde, Anna E Böhmer, Wei Tian, William R Meier, Bing Li, Benjamin G Ueland, Mingyu Xu, Sergey L Bud’ko, Paul C Canfield, *et al.*, “Antiferromagnetic order in  $\text{CaK}(\text{Fe}_{1-x}\text{Ni}_x)_4\text{As}_4$  and its interplay with superconductivity,” *Physical Review B* **97**, 224521 (2018).
- [27] H. Suderow, I. Guillamon, and S. Vieira, “Compact very low temperature scanning tunneling microscope with mechanically driven horizontal linear positioning stage,” *Review of Scientific Instruments* **82**, 033711 (2011).
- [28] See Supplemental Material at [URL will be inserted by publisher] for further details on the experimental set-up, results on the superconducting vortex lattice and further details on the density functional calculations.
- [29] Jennifer E Hoffman, “Spectroscopic scanning tunneling microscopy insights into Fe-based superconductors,” *Reports on Progress in Physics* **74**, 124513 (2011).
- [30] O.K. Andersen and L. Boeri, “On the multi-orbital band structure and itinerant magnetism of iron-based superconductors,” *Annalen der Physik* **523**, 8–50 (2011).
- [31] Rafael M Fernandes, Daniel K Pratt, Wei Tian, Jerel Zarestky, Andreas Kreyssig, Shibabrata Nandi, Min Gyu Kim, Alex Thaler, Ni Ni, Paul C Canfield, *et al.*, “Unconventional pairing in the iron arsenide superconductors,” *Physical Review B* **81**, 140501 (2010).
- [32] A Kreyssig, MG Kim, S Nandi, DK Pratt, W Tian, JL Zarestky, N Ni, A Thaler, SL Bud’ko, PC Canfield, *et al.*, “Suppression of antiferromagnetic order and orthorhombic distortion in superconducting  $\text{Ba}(\text{Fe}_{0.961}\text{Rh}_{0.039})_2\text{As}_2$ ,” *Physical Review B* **81**, 134512 (2010).
- [33] Huiqian Luo, Rui Zhang, Mark Laver, Zahra Yamani, Meng Wang, Xingye Lu, Miaoyin Wang, Yanchao Chen, Shiliang Li, Sung Chang, *et al.*, “Coexistence and competition of the short-range incommensurate antiferromagnetic order with the superconducting state of  $\text{BaFe}_{2-x}\text{Ni}_x\text{As}_2$ ,” *Physical review letters* **108**, 247002 (2012).
- [34] J Munevar, H Micklitz, J Agüero, Guotai Tan, Chenglin Zhang, Pengcheng Dai, and E Baggio-Saitovitch, “Superconductivity and antiferromagnetism in  $\text{Ba}_{0.75}\text{K}_{0.25}\text{Fe}_2\text{As}_2$  single crystals as seen by  $^{57}\text{Fe}$  Mössbauer spectroscopy,” *Physical Review B* **88**, 184514 (2013).
- [35] Kazushige Machida, “Spin density wave and superconductivity in highly anisotropic materials,” *Journal of the Physical Society of Japan* **50**, 2195–2202 (1981).
- [36] R. M. Fernandes, S. A. Kivelson, and E. Berg, “Vestigial chiral and charge orders from bidirectional spin-density waves: Application to the iron-based superconductors,” *Phys. Rev. B* **93**, 014511 (2016).
- [37] Sudip Chakravarty, “Theory of the d-density wave from a vertex model and its implications,” *Phys. Rev. B* **66**, 224505 (2002).
- [38] H. J. Schulz, “Fermi-surface instabilities of a generalized two-dimensional Hubbard model,” *Phys. Rev. B* **39**, 2940–2943 (1989).
- [39] Sudip Chakravarty, R. B. Laughlin, Dirk K. Morr, and Chetan Nayak, “Hidden order in the cuprates,” *Phys. Rev. B* **63**, 094503 (2001).
- [40] Serafim Teknowijoyo, Kyuil Cho, M Kończykowski, Erik I Timmons, Makariy A Tanatar, William R Meier, Mingyu Xu, Sergey L Bud’ko, Paul C Canfield, and Ruslan Prozorov, “Robust  $s\pm$  pairing in  $\text{CaK}(\text{Fe}_{1-x}\text{Ni}_x)_4\text{As}_4$  ( $x=0$  and  $0.05$ ) from the response to electron irradiation,” *Physical Review B* **97**, 140508 (2018).